Published in final edited form as:
Organometallics. 2012 March 26; 31(6): 2231–2243. doi:10.1021/om2011694.

Dinickel Bisphenoxyiminato Complexes for the Polymerization of Ethylene and α-Olefins

Madalyn Radlauer, **Michael W. Day**, and **Theodor Agapie**
Division of Chemistry and Chemical Engineering, California Institute of Technology, Pasadena, California, 91125

Abstract

Dinuclear nickelphenoxyiminato olefin polymerization catalysts based on rigid *p*-terphenyl frameworks are reported. Permethylation of the central arene of the terphenyl unit and oxygen substitution of the peripheral rings *ortho* to the aryl-aryl linkages blocks rotation around these linkages allowing atropisomers of the ligand to be isolated. The corresponding *syn* and *anti* dinickel complexes (**25-s** and **25-a**) were synthesized and characterized by single crystal X-ray diffraction. These frameworks limit the relative movement of the metal centers restricting the metal-metal distance. Kinetics studies of isomerization of a ligand precursor (**7-a**) allowed the calculation of the activation parameters for the isomerization process ($\Delta H^{\ddagger} = 28.0 \pm 0.4$ kcal×mol^{-1} and $\Delta S^{\ddagger} = -12.3 \pm 0.4$ cal×mol^{-1}×K^{-1}). The reported nickel complexes are active for ethylene polymerization [TOF up to 3700 (mol C_2H_4)×(mol Ni)$^{-1}$×h^{-1}] and ethylene/α-olefin copolymerization. Only methyl branches are observed in the polymerization of ethylene, while α-olefins are incorporated without apparent chain walking. These catalysts are active in the presence of polar additives and in neat tetrahydrofuran. The *syn* and *anti* isomers differ in polymerization activity and polymer degree of branching and molecular weight. For comparison, a series of mononuclear nickel complexes (**26**, **27-s**, **27-a**, **28**, **30**) was prepared and studied. The effects of structure and catalyst nuclearity on reactivity are discussed.

Introduction

In recent years, a variety of multinuclear polymerization catalysts have been developed.[1] These systems are conceptually inspired by enzyme active sites, which often contain a multimetallic core. For example, in hydrolases and lyases Lewis acidic metal centers cooperatively activate substrates to facilitate catalysis.[2–4] In search of catalysts with enhanced olefin polymerization abilities, complexes incorporating two potential polymerization sites have been synthesized and investigated. Compared to monometallic analogs, many of these bimetallic systems have been reported to incorporate higher levels of bulky comonomers in copolymerizations with ethylene.[5–10] For dinuclear catalysts based on late metals, increased incorporation of polar monomers has been observed.[1] However, these favorable properties are not general and some systems are reported to have decreased polymerization activities.[11] Further studies are necessary to gain a detailed understanding of how bimetallic cooperativity can be achieved and controlled to generate desirable polymers.

Multinucleating ligands are commonly used to organize metal centers near each other. Cyclopentadienyl, phenoxide, amide, imine, pyridine, and other neutral and anionic donors have been utilized as part of such multinucleating ligand architectures.[1] Typically, two

Supporting Information Available: Experimental procedures and characterization for compounds **1**, **9**–**30**, characterization data for polymers, kinetic plots, and crystallographic details for **25-s** and **25-a**. This material is available free of charge via the internet at http://pubs.acs.org.

identical moieties known to support olefin polymerization catalysis are connected via a linker. The nature of the linker varies from flexible, saturated alkyl chains to unsaturated olefins, arenes, biphenyls, and rigid ring systems. The type and position of the linker controls the relative orientation of the metals and the dynamics of the catalyst.

The nickel phenoxyiminato system represents a well-studied catalyst family.[12] These catalysts are highly active for ethylene polymerization, and the incorporation of other monomers has been reported. Notably, polymerizations can be performed in the presence of polar additives such as ethers and amines.[13] Addition of such bases poisons classical early metal catalysts. Examples of ethylene polymerizations performed in aqueous emulsions are common with nickel phenoxyiminato catalysts.[14–17]

Partly due to the catalytic versatility and ease of synthesis of nickel phenoxyiminato systems, bimetallic versions have been developed (Chart 1).[7,11,17–24] In these systems, the two nickel centers are linked via either the imine donor (**a**, **b**, **e**, **f, g**), the phenoxide donor (**d**, **h**), or both (**c**). The measured or proposed Ni–Ni distance varies from 3.1 Å (**h**) to between 7.5–8.5 Å (**c**, **d**, **e**, and **f**).[11,18,19,21–24] Analysis of the solid-state structures highlights the challenge in orienting the metal centers such that they would react cooperatively with substrates. For some of the reported systems the metals are found in geometries that make intramolecular cooperativity unlikely. For example, system **f** places the metal centers *anti* with respect to the aromatic linker.[22] In system **d**, the coordination planes of the nickel centers are oriented at dihedral angles slightly higher than 90°, and the polymerization sites of each metal are directed away from the other metal.[24] In **c**, the nickel coordination planes are almost parallel which may be a favorable orientation for cooperative binding of substrate, but the two sites involved face in opposite directions.

The dinuclear complexes in Chart 1 differ from their mononuclear counterparts in some aspects of catalytic behavior.[7,11,17–24] With systems **a** and **b**, ethylene polymerization activities are similar to mononuclear controls, but enhanced comonomer incorporation and activity occur in the copolymerization of ethylene with functionalized norbornene derivatives.[19,20] When activated with MAO, system **e** produces polymer with higher M_w than some previously reported mononuclear systems.[21] Complex **f** (R = Ph) shows increased ethylene polymerization activity compared to a mononuclear system studied under the same conditions and produces polymers with higher M_w, but broader molecular weight distributions.[22] The differences between the mono and dinuclear systems were attributed to potential electronic communication of the nickel centers through the ligand bridge in the bimetallic complex.[22] Further investigation of variants of **f** indicates similar tolerance for functional groups as compared to mononuclear counterparts.[23] System **g** displays higher ethylene polymerization activity and produces polymers with increased M_w relative to the mononuclear systems studied.[17] Increased incorporation of comonomers and, most notably, of polar olefins occurs with system **h** relative to mononuclear analogues.[11] The bimetallic effects in systems **a**, **b** and **h** were proposed to involve coordination of the same monomer to both metal centers due to their spatial proximity.[11,20]

The ligand frameworks above highlight a strategy for synthesizing complexes with a fixed metal-metal distance – the linker must be rigid and the coordination sites involved in polymerization accessible from the same direction for both metals. To access a family of dinickel complexes that would allow for studies of the effect of the Ni–Ni distance and orientation of the metal coordination plane, we developed a ligand framework based on a terphenyl moiety, with blocked rotation around aryl-aryl bonds due to ring substitution. The synthesis of dinickel and mononickel complexes supported by this ligand architecture is reported herein along with polymerization and copolymerization studies with a variety of olefins.

Results and Discussion

Synthesis of binucleating salicylaldimine ligands

The synthesis of the binucleating ligands is based on well-documented procedures. 2-Bromo-4-*tert*-butyl-anisole (**1**) and 1,4-dibromo-2,3,5,6-tetramethylbenzene (**2**) starting materials were made using published syntheses.[25–27] Lithium-halogen exchange of **1**, followed by treatment with $ZnCl_2$ afforded an aryl-zinc reagent suitable for a double Negishi cross-coupling with **2**. The palladium-catalyzed coupling reaction led to a mixture of two atropisomers, *syn* (**3-s**) and *anti* (**3-a**). Bromination of **3** with Br_2 *ortho* to the methoxy groups generated dibromide **4**. Column chromatography was used to separate the two atropisomers, which were then carried forward to the final ligand precursors, **7-s** and **7-a**, by the same synthetic procedures. Lithium-halogen exchange followed by addition of excess *N,N*-dimethylformamide (DMF) provided the diformyl species **5** upon aqueous work-up. Removal of the methyl protecting groups was accomplished with excess BBr_3 to afford compounds **6**. Condensation with aniline generated the binucleating ligand precursors **7**. The syntheses were high yielding overall: approximately 40% yield for the *anti*-analog (**7-a**) and 25% yield for the *syn*-analog (**7-s**).

Synthesis of mononucleating salicylaldimine ligands based on biphenyl and terphenyl frameworks

For comparison with the dinuclear systems, mononucleating ligands were also prepared. Several aspects of the terphenyl framework were investigated. The steric effect close to the metal center was tested by targeting catalysts based on a salicylaldimine substituted with pentamethylphenyl *ortho* to the oxygen (**13**). A previously reported variant (**29**)[28] of this ligand includes a phenyl group instead of pentamethylphenyl and was studied as a more sterically open version of **13**. Dinucleating ligand precursors **7-s** and **7-a** bear steric bulk on both peripheral rings of the terphenyl unit. Three mononucleating terphenyl ligands were prepared to mimic the remote steric environment of **7-s** and **7-a**. All are fully substituted on the central ring. Two have oxygen substitution on both peripheral aryls in the position *ortho* to the central ring. This substitution pattern blocks the aryl-aryl rotation and leads to *syn* and *anti* isomers (**19-s** and **19-a**, respectively). The third mononucleating terphenyl ligand (**24**) has 3,5-di-*tert*-butyl substitution on the second peripheral ring.

The synthesis of salicylaldimine **13** was accomplished in five steps (Scheme 2). Negishi cross-coupling of **1** and pentamethylbromobenzene[29] afforded biphenyl species **9**. Subsequent steps are similar to the synthesis of ligands **7-s** and **7-a**. Bromination, followed by lithium-halogen exchange and DMF treatment installed the formyl moiety to give **11**. Deprotection of the ether group and condensation with 2,6-diisopropyl aniline provided **13** in 14% overall yield.

The synthesis of the mononucleating terphenyl ligand analogs was accomplished via a modification of the procedure in Scheme 1. Negishi cross-coupling of **2** with 2.2 equivalents of zinc reagent stemming from methoxymethyl (MOM)-protected 2-bromo-4-*tert*-butylphenol afforded both the expected terphenyl species as well as a bromo-substituted biphenyl species **15** (Scheme 3). The isolation of the mono-cross-coupled product (**15**) was instrumental to the preparation of asymmetric terphenyl ligands. A second cross-coupling, with orthogonally protected 2-bromo-4-*tert*-butylanisole (**1**), afforded the *syn* and *anti* atropisomers of terphenyl species **16** in a ratio of 1:1. Deprotonation directed by the MOM-protected ether using *n*-butyllithium and *N,N,N′,N′*-tetramethylethylenediamine (TMEDA) led, upon reaction with DMF and aqueous workup, to the installation of a single formyl group. Acid-catalyzed removal of the MOM group followed by condensation with 2,6-diisopropylaniline afforded **19-a** and **19-s** in 35 and 37% yield, respectively, starting from

compounds **16**. Separation of the two atropisomers was accomplished by column chromatography after the second Negishi cross-coupling (compounds **16**). The third mononucleating terphenyl ligand was synthesized starting from the Negishi cross-coupling of **15** with the aryl-zinc reagent derived from 3,5-di-*tert*-butylbromobenzene to yield asymmetric terphenyl **21** (Scheme 4). Adapting the protocols from the synthesis of **19**, **21** was converted to monophenol **24** in 34% overall yield from **15**. A single isomer is expected because of the lack of substitution *ortho* to the central ring and due to the symmetrical substitution pattern on the peripheral aryl.

Studies of the interconversion of atropisomers

In the context of preserving the steric environment and the metal-metal separation in complexes supported by ligands with restricted rotation around aryl-aryl bonds, it is of interest to determine the kinetic and thermodynamic behavior of the atropisomers. Because the nickel complexes decompose before isomer interconversion (*vide infra*), kinetics studies of the interconversion of ligand precursor **7-a** to **7-s** were performed in [D_0]-1-bromonaphthalene at 140, 150, 160 and 170 °C and were monitored by ^{1}H NMR spectroscopy. Starting from either **7-s** or **7-a**, equilibrium was reached over 20 h at 140 °C, 8 h at 150 °C, 3.5 h at 160 °C, and 1.75 h at 170 °C. At these temperatures, the equilibrium constant is K_{eq} = [**7-s**]/[**7-a**] = 0.61 (eq 1). The studied processes fit the integrated rate expression for approach to equilibrium of first-order kinetics (eq 2; X_e = concentration at equilibrium; X = concentration at time t) (see SI).[30] An Eyring plot using the determined rate constants provided activation energy parameters: $\Delta H^{\ddagger}$ = 28.0 ± 0.4 kcal×mol^{-1} and $\Delta S^{\ddagger}$ = −12.3±0.4 cal×mol^{-1}×K^{-1} (Figure 1). As expected, the calculated free energy barrier to rotation for **7-a** ($\Delta G^{\ddagger}$ = 32 kcal×mol^{-1} at 298 K) is significantly higher than for a recently reported terphenyl system without permethylation of the central arene (14.6 kcal×mol^{-1}).[31] Although the entropy of activation for conformational dynamic processes is typically close to zero, the larger absolute value determined here is still in the range reported for related fluxional processes, for example rotation around the C–NMe_2 bond of a N,N-dimethylthiourethane ($\Delta S^{\ddagger}$ = −8±2 cal×mol^{-1}×K^{-1}).[32] The significantly negative value suggests a relatively ordered transition state likely corresponding to the geometry with two aryl rings coplanar. This geometry may require significant distortions of the ring substituents. The barrier for isomerization for **7-a** is comparable to the reported value for the restricted rotation in hexaarylbenzenes (ca. 33 kcal×mol^{-1} at 419 K).[33] Extrapolating to 25 °C (the temperature at which most of the polymerizations discussed herein were run), the rate constant for the interconversion of **7-a** and **7-s** is approximately 10^{-11} s^{-1} indicating that virtually no isomerization takes place over the course of the polymerization experiment.

$$\mathbf{7-a} \underset{k_{sa}}{\overset{k_{as}}{\rightleftarrows}} \mathbf{7-s} \quad (1)$$

$$\ln(X_e - X) = -(k_{as}+k_{sa}) \bullet t \quad (2)$$

Synthesis of nickel complexes

Nickel complexes were prepared via alkane elimination. Reaction of phenols with a 10% excess of $NiMe_2$(tmeda) in diethyl ether in the presence of excess pyridine allowed for the isolation of the nickel-methyl species supported by the corresponding phenoxyiminato ligands with a bound pyridine. If acetonitrile or tertiary amine (*N,N*-dimethylbutylamine or *N,N*-dimethylethylamine) were utilized instead of pyridine or if no additional labile ligand was added, the desired nickel complexes were not isolated cleanly. The ^{1}H NMR spectra of

the isolated nickel complexes each display a single peak around −0.5 ppm, diagnostic for the Ni-CH_3 moiety. The atropisomers were assigned by ^{1}H-^{1}H NOESY and ROESY NMR studies. Through-space cross peaks are observed between the *meta* proton of the Ni-bound pyridine and the proton *ortho* to the aryl-aryl linkage for only one of the isomers (see SI). This isomer was assigned as the *anti* atropisomer (**25-a** and **27-a**).

NMR spectra of the nickel complexes are each indicative of a single ligand environment, suggesting that for complexes with atropisomers no isomerization occurs during synthesis. Heating solutions of **25-s** and **25-a** in benzene at 50 °C for 13 h did not cause isomerization of **25-s** to **25-a** or **25-a** to **25-s**, respectively (^{1}H NMR spectroscopy). No decomposition was observed for **25-a**, though 70% decomposition of **25-s** was observed, based on the disappearance of the Ni-CH_3 peak in the ^{1}H NMR spectrum. Heating of **25-s** and **25-a** at 70 °C for 8 h led to 100% and 10% decomposition, respectively, but no isomerization. Further heating of **25-a** at 90 °C for 12 h caused significant decomposition, but no isomerization to **25-s**. Analogous results were seen when heating **27-a** and **27-s** to 90 °C for 6 h resulting in about 60% decomposition of **27-s** and 80% decomposition of **27-a**. These studies indicate that the energetic barrier is too high for isomerization to occur at any appreciable rate at 25 °C, consistent with the kinetics studies completed with the bis-salicylaldimines **7-a** and **7-s** (*vide supra*).

Structure of dinickel complexes

X-ray quality single crystals were obtained from a concentrated pentane solution cooled at −35 °C for **25-s** and by vapor diffusion of hexanes into tetrahydrofuran at room temperature for **25-a**. X-ray diffraction studies provided structural confirmation of the identity of the isomers (Figure 2) as assigned by NMR spectroscopy above. The methyl groups are located *trans* to the phenoxide and the pyridine *trans* to the imine, as reported for similar coordination environments.[34] The Ni-Ni distance is 7.1 Å (average for the two molecules in the asymmetric unit) for the *syn* isomer (**25-s**). A slight distortion from square planar geometry is observed, probably due to the pyridine ligands that extend towards each other and must tilt to avoid steric interaction. The planes of the two pyridines are about 3.86 Å apart, possibly indicative of a weak **π** interaction.[35] The direction of binding of the pyridine ligands indicates that appropriate substrates may reach both metal centers for cooperative interaction. Conversely, for the *anti* atropisomer (**25-a**) intramolecular cooperativity is not possible because of the large metal-metal distance (11.1 Å), and because the nickel centers are on opposite faces of the central arene ring. The N(1)-Ni(1)-N(2) and N(3)-Ni(2)-N(4) angles in the syn isomer of 173° and 166°, respectively (average for the two molecules in the asymmetric unit), and the N(1)-Ni(1)-N(2) angle of 177° in the *anti* isomer is nearly linear. Ni-N, Ni-O, and Ni-Me distances are similar to known complexes.[19,22,28,34,36,37]

Ethylene polymerization

Ethylene homopolymerization trials were performed to determine the effect of reaction scale, reaction time, catalyst loading, and solvent (Table 1). Duplicate polymerization trials show changes in turnover frequencies (TOF) of less than 50% in the majority of cases. Increased reaction time led to increased polymer yield indicating that the catalyst remains active over extended periods (e.g. entries 3, 4, 5, Table 1). Ethylene polymerizations in 25 mL of toluene with **25-a** and mononuclear counterparts **26**, **27-a**, **28**, and **30** resulted in similar catalytic activities (TOFs 1200–3700 (mol C_2H_4)×(mol Ni)$^{-1}$×h^{-1}) (e.g. entries 3, 18, 23, 33, 37, Table 1). This level of activity is similar or lower than seen with nickel salicylaldimines that have a phosphine or nitrile ligand in place of the pyridine, which may be due in part to the stability of the pyridine-bound complex.[13] The highest TOFs were observed using **25-a** and **26** (entries 3,18, Table 1). **25-s** exhibits catalytic activity one order of magnitude less than **25-a** (entries 10–13, Table 1), and is generally less active than the

other investigated catalysts. Similarly, **27-s** has activity three-fold lower than **27-a** (entries 28, 29, Table 1). The observed difference in TOFs between **25-s** and **25-a** may be due to the effect of crowding of the catalytic pocket by the second nickel center. Similarly, steric bulk on the remote aryl of the terphenyl unit may be responsible for the difference between **27-s** and **27-a**.

Decreasing the scale of the polymerization reaction by five times (5 mL toluene) caused a significant drop in activity (e.g. entry 4 versus entry 7, Table 1). The concentration of nickel complex was doubled in order to collect enough polymer for analysis when running polymerizations at this scale. These changes in scale and concentration resulted in a reduction of TOF by two- to ten-fold (entries 4, 7; 12–15; 18–20; 23–25; 28–30; 33, 34; 37, 38, 40; Table 1). This effect is not well understood, but may be caused by changes in mixing of the solution and mass transfer problems, which could lower the effective concentration of ethylene in solution. To test the effect of mixing, a polymerization with **25-a** was run with stirring at one third the rate used for all other polymerizations (entry 6, Table 1). The TOF in this polymerization was reduced by two-fold from an identical trial with the higher stirring rate (entries 4, 6, Table 1), supporting the hypothesis that insufficient mixing in the smaller scale polymerizations could contribute to the drop in activity. Changing the solvent from toluene to tetrahydrofuran (THF), did not significantly affect the activity of **25**–**28**, but decreased the activity of **30** by four-fold (entries 7–9; 14–17; 20, 21; 30–32; 34–36; 40–42; Table 1). This drop in activity for **30** is similar to the three- to five-fold drop in TOF reported for polymerizations with phosphine-ligated nickel salicylaldimine complexes in the presence of excess ethers.[11,13,23] The notable lack of inhibition by THF of catalysts **25**–**28** may be due to the steric bulk of the fully substituted aryl group *ortho* to oxygen disfavoring ether coordination.

Polymer characterization by ^{1}H and ^{13}C NMR spectroscopy showed only methyl branch formation with peaks in the D_2-tetrachloroethane ^{13}C NMR spectrum at δ 20.1, 27.5, 30.4, 33.4 and 37.6 ppm assigned to the methyl branch carbon, the β carbon, the γ carbon, the methyne carbon and the α carbon, respectively.[38] The variation in polymer branching level (determined by ^{1}H NMR spectroscopy) was less than 35% for repeated trials, indicating good reproducibility.[39,40] Polymers resulting from **25-s** have the highest level of branching by at least two-fold compared to products from other catalysts under the same catalytic conditions (up to 70 branches/1000 C, entry 16, Table 1). Increase in polymer branching was also observed upon the combination of scale reduction, catalyst concentration increase, and the solvent change to THF (e.g. compare entries 12, 16, Table 1). Polymer branching is caused by chain walking processes that are dependent on relative rates of olefin insertion and β-H elimination/isomerization.[41–44] Increased ethylene concentration allows for faster olefin insertion compared to isomerization and leads to lower levels of branching. Higher branch density in the small-scale experiments is consistent with lower concentration of monomer due to inefficient mixing (as proposed for the decreased yield) and with the lower solubility of ethylene in THF.

The selectivity for methyl branches is notable. Previously reported dinuclear nickel polymerization catalysts based on system **h** (Chart 1) also generate polyethylene with only methyl branches and there are a few additional accounts of dinuclear nickel systems producing polyethylene with predominantly methyl branches.[7,11] This contrasts with previously reported mononickel systems that show longer branches as well.[19,21–24] Catalysts **25**–**28** and **30** generate polyethylene with only methyl branches (path **A**, Scheme 6) suggesting that the proximal ligand environments hinder the formation of ethyl (or longer) branches regardless of the contributions from a second metal center. Bulky ligands can disfavor path **B** in Scheme 6, which involves species with nickel bound to a secondary carbon substituted with an ethyl group and the polymeryl chain. Similar to system **h**, the

dinuclear *syn* isomer **25-s** generates increased branch density compared to the mononuclear analogs. One explanation invokes slower propagation kinetics for **25-s** compared to **25-a** and the mononuclear systems, allowing for more extensive chain walking with **25-s**. In THF, compound **27-s** produced polymers with lower branching despite similar TOFs compared with **25-s** (entries 16, 17, 31, 32, Table 1); this behavior suggests that the simple ligand sterics explanation is not fully satisfactory. However, a direct bimetallic interaction of pendant C–H bonds in the chain walking intermediates, as proposed for **h**, seems unlikely given the significant metal-metal distance.

Ethylene/1-hexene copolymerization

Ethylene/1-hexene copolymerization trials were also performed to determine the effects of reaction scale, comonomer concentration, reaction time, reaction temperature and solvent on the resultant copolymers (Table 2). As with the ethylene homopolymerizations, polymerizations with **25-s** and **27-s** produced the least polymer, and polymers synthesized using **25-s** display the largest amount of branching (e.g. entries 6, 16, 18, 21, 24, 27, 29, Table 2). The change in activity from homopolymerizations of ethylene observed in experiments performed on a 25 mL scale (Table 1, entry 1 versus Table 2, entry 1) was one order of magnitude matching previous reports of one order of magnitude decrease in activity from ethylene homopolymerization upon addition of an α-olefin comonomer in large excess.[36] The drop observed on a 5 mL scale, however, was not as significant (only up to 4.4 times). The decrease in activity was previously explained by a slower insertion rate of the α-olefins.[16,36] As expected, lower comonomer concentration led to higher TOF (Table 2 entries 4 and 5). Extension of the reaction time from 3 to 12 h resulted in a lowered TOF, presumably due to catalyst decomposition over time. Increasing the temperature resulted in a less than twofold decrease in activity in 3 h polymerization reactions and approximately no change in activity in 12 h polymerization runs (Table 2, entries 8 and 11 and entries 10 and 12). Change of solvent also had negligible effect on either the yield or the branching of the resultant polymers. Overall, the behavior of catalysts **25-a**, **25-s**, **26**, **27-a**, **27-s**, **28**, and **30** is comparable to previously reported monometallic systems.[16,36] A noteworthy trend is the higher branching with the *syn* catalysts **25-s** and **27-s**; this may also be a consequence of the bulkier environment, which slows propagation compared to chain walking. Additionally, all of the polymers characterized by ^{13}C NMR spectroscopy displayed only methyl and butyl branches, which is a unique microstructure. Further study of this phenomenon was accomplished by polymerization trials with other α-olefins.

Ethylene/α-olefin copolymerization

Ethylene/α-olefin copolymerization trials were performed in duplicate with **25-a** and **25-s** and 1-pentene, 1-hexene, 1-heptene, and 1-octene to evaluate the effects of nickel-nickel proximity on branching, comonomer incorporation, TOF, molecular weight and molecular weight distribution (Table 3). Again, significantly more branching was observed in polymers produced with **25-s** than in polymers produced with **25-a**, but the percent incorporations of 1-pentene and 1-hexene were similar. This behavior suggests that the difference in the extent of branching was due to the presence of additional methyl branches from chain walking rather than to the incorporation of additional comonomer. With the longer α-olefins, 1-heptene and 1-octene, a greater degree of comonomer incorporation was seen in polymers generated by **25-a** than by **25-s**, likely due to increased steric hindrance in **25-s**.

In all of the ethylene/α-olefin copolymers examined by ^{13}C NMR spectroscopy (Tables 2 and 3), only isolated methyl branches and branches the length of the comonomer chain were present. These data suggest that chain walking along the polyethylene chain to methyl branches occurs, but that after the insertion of a comonomer, no chain isomerization takes place before the coordination and insertion of the next ethylene monomer (paths **C** and **D**,

Scheme 6; Scheme 7). To the best of our knowledge, this type of polymer microstructure has not been previously reported for ethylene-α-olefin copolymerization; it formally corresponds to an ethylene-propylene-α-olefin copolymer, without chain walking.[16,36] Mecking *et al.* specifically report a variety of branch lengths including methyl, ethyl and butyl branches in the copolymerization of ethylene and 1-butene, which are attributed to various modes of insertion and subsequent chain walking.[16] Assuming 1,2-insertions are favored (paths **D** and **F**, Scheme 6), the difference in polymer microstructure achieved in polymerizations with the current systems may arise from the steric hindrance caused by the supporting ligand, disfavoring path **F** in which nickel migration to a tertiary carbon from a primary one.[15,45,46]

GPC analysis was performed on several of the ethylene/α-olefin copolymers (Table 3). In all cases, the molecular weights of polymers produced with **25-a** were higher than of polymers produced with **25-s**. The molecular weights for polymers produced with both **25-a** and **25-s** generally decreased with increasing comonomer size. The PDI values were between 3 and 4 except for the homopolymerization of ethylene with **25-a** (PDI=7.5). Generally, lower PDI values were observed for **25-s** compared to **25-a**. The observed molecular weights and PDIs are in the range previously reported for mono- and dinickel catalysts.[7,13,19,20,34] Notably, high PDIs (5–8) were reported previously for bimetallic catalysts (**c**, **f** Chart 1).[19,22] The difference in polymer molecular weight is indicative of the relative rates of propagation vs chain termination, which depend on the rates of olefin insertion and β-H elimination, respectively.[47] The lower molecular weights for **25-s** vs **25-a** contrast with previous reports of a bimetallic catalsyt leading to an increase in M_w vs the monometallic version,[22] but are consistent with the trends in TOF and branching level. Compared to **25-a**, complex **25-s** displays lower TOF and higher branching consistent with lower olefin insertion rates and higher β-H elimination rates, which is in agreement with the observed lower molecular weight polymers. Similar agreement between trends of M_w vs TOF and polymer branching (for **25-a**) were observed upon variation of the comonomer. The larger comonomers may lead to lower insertion rates due to steric reasons and result in lower M_w polymers.[16,36]

Copolymerizations of ethylene and polar monomers were also attempted. Using a large excess of a comonomer with a distal polar moiety, ethyl undecylenate (Table 4, entries 21 and 22; 2500 equivalents per nickel), led to a modest yield of polymer and incorporation within the range of previous reports for related catalysts.[36] Copolymerization attempts with 225 equivalents of *N,N*-dimethylallylamine per nickel resulted in polyethylene with no polar comonomer incorporation observed by ^1H or ^{13}C NMR spectroscopy, but larger inhibitory effects for **25-a** compared to **25-s**.[48] In contrast, copolymerization attempts with 225 equivalents of methyl acrylate per nickel resulted in no observable polymer. These data indicate that **25-a** and **25-s** tolerate some polar monomers. Additional investigations of the copolymerization of ethylene and polar monomers with these complexes are ongoing.

Conclusions

The *syn*- and *anti*-atropisomers of a dinuclear neutral nickel bisphenoxyiminato complex (**25**) were synthesized and characterized. Kinetic studies of the bis-salicylaldimine precursors (**7**) indicate that virtually no isomerization between the *syn* and *anti* atropisomers occurs at 25 °C, making these terphenyl complexes suitable for the systematic study of the effects of metal-metal cooperativity. The terphenyl dinuclear complexes polymerize ethylene similarly to previously reported mononickel salicylaldimine complexes such as **30**. Ethylene polymerization leads to polyethylene with only methyl branches. Copolymerizations of ethylene and α-olefins with complexes **25, 26, 27, 28** and **30** produce polyethylene with methyl branches and branches the length of the comonomer side-chain

(three to six carbons depending on the comonomer). This polymer microstructure has not been previously reported, to our knowledge, for the copolymerization of ethylene and α-olefins with nickel salicylaldiminato catalysts. Complexes **25–28** retain polymerization activity in the presence of an excess of polar additives such as THF, in contrast to the decreased activity of complex **30**. Because no nickel-nickel cooperativity is expected in **25-a** or the mononuclear complexes, this tolerance is attributed to the steric environment of the permethylated arene that is not present in **30**. While no polymer was produced in attempted copolymerizations of ethylene with methyl acrylate, copolymerizations of ethylene with an olefin possessing a distal polar moiety is observed, indicating some functional monomer tolerance for **25-s** and **25-a**. Generally, the *syn* catalysts were found to be less active and generate lower M_w polymers than the *anti* analogs. More branching is observed for the *syn* catalysts. These effects are explained in terms of increased steric bulk. This steric effect is currently exploited for polymerizations in the presence of strong Lewis bases that would significantly deactivate the nickel catalysts in the absence of a compensating bimetallic effect.[48] Although large differences between the *syn* and *anti* dinuclear catalysts reported here have not been observed, the present systems provide a robust framework amenable for further studies of dinuclear catalysts for olefin polymerization. Future investigations include changing the relative position of the two metal centers on the terphenyl moiety, the nature of the metals, and the donor sets.

Experimental Section

General Considerations

All air- and/or water-sensitive compounds were manipulated using standard vacuum or Schlenk line techniques or in an inert atmosphere glove box. The solvents for air- and moisture-sensitive reactions were dried over sodium benzophenone ketyl, calcium hydride, or by the method of Grubbs.[49] All NMR solvents were purchased from Cambridge Isotopes Laboratories, Inc. Benzene-d_6 was dried over sodium benzophenone ketyl and vacuum transferred prior to use. 1-Bromonaphthalene, pyridine, 1-pentene, 1-hexene, 1-heptene, 1-octene, ethyl undecylenoate, N,N-dimethylallylamine, and methyl acrylate were dried over calcium hydride and vacuum transferred prior to use. Ethylene was purchased from Matheson and equipped with a PUR-Gas in line trap to remove oxygen and moisture before use. All ^{1}H, ^{13}C, and 2D NMR spectra of small organic and organometallic compounds were recorded on Varian Mercury 300 MHz, Varian 400 MHz, or Varian INOVA-500 or 600 MHz spectrometers at room temperature. All ^{1}H and ^{13}C NMR spectra of polymers were recorded on the Varian INOVA-500 MHz spectrometer at 130 °C. Chemical shifts are reported with respect to residual internal protio solvent. 2-bromo-4-*tert*-butylphenol,[25] **2**,[27] **8**,[29] chloromethyl methyl ether,[50] Ni(acac)$_2$(tmeda),[51] NiMe$_2$(tmeda),[52] and 3-phenyl salicylaldehyde[53] were synthesized according to literature procedures.

3—Synthesis of these terphenyl compounds was accomplished via the Negishi coupling of 1,4-dibromo-2,3,5,6-tetramethylbenzene (**2)** with two equivalents of 2-bromo-4-*tert*-butylmethoxybenzene (**1**).[55] In the glove box, **1** (25.44 g, 104 mmol, 1 equiv) and 250 mL of THF were combined in a large Schlenk tube and frozen in the cold well. ^{t}BuLi (1.7 M solution in pentane, 129 mL, 219 mmol, 2.1 equiv) was added to the thawing solution and stirred for 1 h while warming to room temperature. The resultant yellow orange solution was refrozen in the cold well. Concurrently, a suspension of $ZnCl_2$ (9.98 g, 73 mmol, 0.7 equiv) in THF (100 mL) was frozen in the cold well. The thawing $ZnCl_2$ suspension was added to the thawing reaction mixture and stirred for 1 h resulting in a colorless cloudy solution. **2** (13.75 g, 47. mmol, 0.45 equiv), Pd(PPh$_3$)$_4$ (1.21 g, 1.1 mmol, 0.01 equiv) and THF (100 mL) were added to the reaction mixture at room temperature. The sealed Schlenk tube was brought out of the glove box and heated to 75 °C for 5 days. Water was added to quench the

reaction. The solution was filtered over silica gel and the silica gel was washed with dichloromethane (DCM). The two atropisomers of the terphenyl compound were coprecipitated from methanol as a colorless solid (15.4 g, 71% yield). ^{1}H NMR (300 MHz, $CDCl_3$): δ 7.36 (2dd, 2H, Ar*H*), 7.19 (2d, 2H, Ar*H*), 6.95 (2d, 2H, Ar*H*), 3.78 (2s, 6H, OCH_3), 1.99 (2s, 12H, ArCH_3), 1.34 (2s, 18H, C(CH_3)$_3$) ppm. ^{13}C NMR (75 MHz, $CDCl_3$): δ 154.70 (Ar), 143.25 (Ar), 137.83 (Ar), 137.57 (Ar), 132.22 (Ar), 132.10 (Ar), 130.75 (Ar), 129.31 (Ar), 128.97 (Ar), 124.29 (Ar), 124.21 (Ar), 110.19 (Ar), 110.09 (Ar), 55.81 (O*C*H$_3$), 55.59 (O*C*H$_3$), 34.29 (Ar*C*(CH$_3$)$_3$), 31.75 (ArC(*C*H$_3$)$_3$), 18.07 (Ar*C*H$_3$), 18.00 (Ar*C*H$_3$) ppm. HRMS (EI+) Calcd. for $C_{32}H_{42}O_2$: 458.3185. Found: 458.3184.

4—Compound **3** (10.00 g, 21.8 mmol, 1 equiv), iron powder (0.0786 g, 1.41 mmol, 0.06 equiv), and 35 mL DCM were combined in a 100 mL round bottom flask equipped with an addition funnel. The flask was covered with foil. Bromine (2.3 mL, 44.7 mmol, 2.05 equiv) and 5 mL of DCM were added to the addition funnel and dripped into the flask over 5 minutes. The reaction mixture was stirred for an additional 3 h at room temperature. The reaction was quenched with aqueous sodium hydrosulfite and sodium carbonate. The desired product was extracted into DCM. The organics were washed with water, dried with $MgSO_4$, filtered and volatiles were removed under vacuum. The two atropisomers were separated by column chromatography (2:1 hexanes/DCM). 8.49 g of white solid were collected of the *anti* isomer and 4.73 g of white solid were collected of the *syn* isomer (overall yield of 98%). **4-a**. ^{1}H NMR (300 MHz, $CDCl_3$): δ 7.56 (d, J = 2.4, 2H, Ar*H*), 7.03 (d, J = 2.4, 2H, Ar*H*), 3.49 (s, 6H, OCH_3), 1.97 (s, 12H, ArCH_3), 1.33 (s, 18H, C(CH_3)$_3$) ppm. ^{13}C NMR (75 MHz, $CDCl_3$): δ 152.09 (Ar), 148.45 (Ar), 137.61 (Ar), 136.84 (Ar), 131.96 (Ar), 129.12 (Ar), 128.40 (Ar), 117.22 (Ar), 60.35 (O*C*H$_3$), 34.66 (Ar*C*(CH$_3$)$_3$), 31.54 (ArC(*C*H$_3$)$_3$), 18.31 (Ar*C*H$_3$) ppm. HRMS (EI+) Calcd. for $C_{32}H_{40}O_2Br^{81}Br$: 616.1374. Found: 616.1376. **4-s**. ^{1}H NMR (300 MHz, $CDCl_3$): δ 7.56 (d, J = 2.4, 2H, Ar*H*), 7.12 (d, J = 2.4, 2H, Ar*H*), 3.38 (s, 6H, OCH_3), 2.00 (s, 12H, ArCH_3), 1.32 (s, 18H, C(CH_3)$_3$) ppm. ^{13}C NMR (75 MHz, $CDCl_3$): δ 151.98 (Ar), 148.49 (Ar), 137.66 (Ar), 136.45 (Ar), 132.41 (Ar), 129.09 (Ar), 128.18 (Ar), 117.33 (Ar), 59.74 (O*C*H$_3$), 34.69 (Ar*C*(CH$_3$)$_3$), 31.50 (ArC(*C*H$_3$)$_3$), 18.22 (Ar*C*H$_3$) ppm. HRMS (EI+) Calcd. for $C_{32}H_{40}O_2Br^{81}Br$: 616.1374. Found: 616.1402.

5-a—Compound **4-a** (5.10 g, 8.28 mmol, 1 equiv) was dissolved in 200 mL of THF in a 500 mL Schlenk flask in the glove box and the solution was frozen in the cold well. ^{t}BuLi (1.7 M in pentane, 20.44 mL, 34.8 mmol, 4.2 equiv) was added in four portions to the cold solution of **4-a**. The reaction turned yellow upon addition of ^{t}BuLi and was allowed to warm to room temperature as it was stirred for 1 h. The reaction mixture was refrozen in the cold well. A solution of DMF (3.84 mL, 49.6 mmol, 6 equiv) in 10 mL of THF was also frozen in the cold well before it was added to the reaction while thawing. The resulting colorless solution was warmed to room temperature and stirred for 2 h. The flask was brought out of the box, and the reaction was quenched with 100 mL of water. Volatiles were removed under vacuum and the desired product was extracted into DCM and washed with brine and water. The organic phase was dried over $MgSO_4$, filtered, and volatile materials were removed under vacuum to give an orange solid. Precipitation from methanol yielded 4.2 g (99% yield) of pale yellow solid. ^{1}H NMR (400 MHz, $CDCl_3$): δ 10.45 (s, 2H, C*H*O), 7.87 (d, J = 2.6, 2H, Ar*H*), 7.35 (d, J = 2.6, 2H, Ar*H*), 3.51 (s, 6H, OCH_3), 2.00 (s, 12H, ArCH_3), 1.34 (s, 18H, C(CH_3)$_3$) ppm. ^{13}C NMR (101 MHz, $CDCl_3$): δ 191.17 (Ar*C*HO), 158.82 (Ar), 147.23 (Ar), 137.22 (Ar), 136.06 (Ar), 135.75 (Ar), 132.34 (Ar), 128.56 (Ar), 123.84 (Ar), 62.16 (O*C*H$_3$), 34.72 (Ar*C*(CH$_3$)$_3$), 31.41 (ArC(*C*H$_3$)$_3$), 18.30 (Ar*C*H$_3$) ppm. HRMS (EI+) Calcd. for $C_{34}H_{42}O_4$: 514.3083. Found: 514.3084.

5-s—The lithium-halogen exchange and formylation of **4-s** was accomplished via the same procedure as the *anti*. The desired product was isolated as a colorless solid in 85% yield (3.4

g). ^{1}H NMR (400 MHz, $CDCl_3$): δ 10.46 (s, 2H, C*H*O), 7.89 (d, J = 2.6, 2H, Ar*H*), 7.45 (d, J = 2.6, 2H, Ar*H*), 3.45 (s, 6H, OC*H*$_3$), 2.05 (s, 12H, ArC*H*$_3$), 1.35 (s, 18H, C(C*H*$_3$)$_3$) ppm. ^{13}C NMR (101 MHz, $CDCl_3$): δ 190.99 (Ar*C*HO), 158.71 (Ar), 147.32 (Ar), 137.34 (Ar), 135.88 (Ar), 135.49 (Ar), 132.78 (Ar), 128.73 (Ar), 123.76 (Ar), 61.40 (O*C*H$_3$), 34.79 (Ar*C*(CH$_3$)$_3$), 31.43 (ArC(*C*H$_3$)$_3$), 18.29 (Ar*C*H$_3$) ppm. HRMS (EI+) Calcd. for $C_{34}H_{42}O_4$: 514.3083. Found: 514.3089.

6-a—BBr_3 (7.74 mL, 81.6 mmol, 10 equiv) was syringed into a Schlenk flask containing a solution of **5-a** (4.20 g, 8.16 mmol, 1 equiv) in 200 mL of DCM under nitrogen atmosphere. The solution turned from yellow to dark red and was stirred for 1.5 h before the reaction was stopped by the gradual addition of water and a color change to dark greenish brown was observed. The desired product was extracted into DCM. The organic phase was dried over $MgSO_4$, filtered, and volatile materials were removed under vacuum to give a greenish brown solid. Trituration with methanol followed by filtration yielded 2.55 g (64% yield) of **6-a** as an olive green solid. ^{1}H NMR (400 MHz, $CDCl_3$): δ 11.12 (s, 2H, O*H*), 9.98 (s, 2H, C*H*O), 7.54 (2s, 4H, Ar*H*), 3.48 (s, 6H, OC*H*$_3$), 1.97 (s, 12H, ArC*H*$_3$), 1.35 (s, 18H, C(C*H*$_3$)$_3$) ppm. ^{13}C NMR (101 MHz, $CDCl_3$): δ 197.20 (Ar*C*HO), 156.69 (Ar), 143.04 (Ar), 137.15 (Ar), 135.92 (Ar), 132.59 (Ar), 131.01 (Ar), 128.78 (Ar), 120.10 (Ar), 34.41 (Ar*C*(CH$_3$)$_3$), 31.44 (ArC(*C*H$_3$)$_3$), 17.93 (Ar*C*H$_3$) ppm. HRMS (EI+) Calcd. for $C_{32}H_{38}O_4$: 486.2770. Found: 486.2784.

6-s—The deprotection of **5-s** was accomplished via the same procedure as the *anti*. The desired product was isolated as a greenish solid in 93% yield (2.95 g). ^{1}H NMR (300 MHz, $CDCl_3$): δ 10.91 (bs, 2H, O*H*), 9.98 (s, 2H, C*H*O), 7.55 (d, J = 2.5, 2H, Ar*H*), 7.45 (d, J = 2.5, 2H, Ar*H*), 3.50 (s, 6H, OC*H*$_3$), 1.98 (s, 12H, ArC*H*$_3$), 1.35 (s, 18H, C(C*H*$_3$)$_3$) ppm. ^{13}C NMR (101 MHz, $CDCl_3$): δ 196.96 (Ar*C*HO), 142.65 (Ar), 136.80 (Ar), 136.22 (Ar), 132.69 (Ar), 130.95 (Ar), 128.79 (Ar), 120.22 (Ar), 34.39 (Ar*C*(CH$_3$)$_3$), 31.47 (ArC(*C*H$_3$)$_3$), 17.95 (Ar*C*H$_3$) ppm. HRMS (EI+) Calcd. for $C_{32}H_{38}O_4$: 486.2770. Found: 486.2785.

7-a—The *anti*-bis-salicylaldimine compound was synthesized by mixing **6-a** (1.5 g, 3.08 mmol, 1 equiv), *p*-toluenesulfonic acid (0.059 g, 0.31 mmol, 0.1 equiv), 2,6-diisopropylamine (1.28 g, 6.78 mmol, 2.2 equiv), and methanol (150 mL) in a round bottom flask equipped with a reflux condenser. A color change from green to orange was observed with the addition of aniline. The mixture was stirred at reflux for 4 h and then cooled to room temperature. A pale orange solid was collected from the red solution via filtration. The precipitate was further purified by column chromatography (7:1 hexanes/DCM) and 1.7 g (68% yield) of pale yellow solid was obtained. ^{1}H NMR (400 MHz, C_6D_6): δ 13.45 (s, 2H, O*H*), 8.05 (s, 2H, NC*H*), 7.42 (d, 2H, Ar*H*), 7.28 (d, 2H, Ar*H*), 7.11 (bs, 6H, N-Ar*H*), 3.06 (septet, J = 6.8, 4H, C*H*(CH$_3$)$_2$), 2.24 (s, 12H, ArC*H*$_3$), 1.29 (s,18H, C(C*H*$_3$)$_3$), 1.06 (d, J = 6.8, 24H, CH(C*H*$_3$)$_2$) ppm. ^{13}C NMR (101 MHz, C_6D_6): δ 168.05 (Ar*C*HN), 157.53 (Ar), 147.32 (Ar), 141.85 (Ar), 138.96 (Ar), 137.61 (Ar), 133.75 (Ar), 132.81 (Ar), 131.98 (Ar), 125.75 (Ar), 123.54 (Ar), 118.49 (Ar), 34.26 (Ar*C*(CH$_3$)$_3$), 31.60 (ArC(*C*H$_3$)$_3$), 28.63 (Ar*C*H(CH$_3$)$_2$), 23.42 (ArCH(*C*H$_3$)$_2$), 18.44 (Ar*C*H$_3$) ppm. HRMS (FAB+) Calcd. for $C_{56}H_{73}O_2N_2$: 805.5672. Found: 805.5693.

7-s—The imine condensation to form the *syn*-bis-salicylaldimine compound from **6-s** was accomplished via the same procedure as the *anti*. The desired product was isolated as a pale yellow solid in 43% yield (1.06 g). ^{1}H NMR (400 MHz, C_6D_6): δ 13.45 (s, 2H, O*H*), 8.06 (s, 2H, NC*H*), 7.45 (d, 2H, Ar*H*), 7.29 (d, 2H, Ar*H*), 7.13 (bs, 6H, N-Ar*H*), 3.12 (septet, J = 6.8, 4H, C*H*(CH$_3$)$_2$), 2.22 (s, 12H, ArC*H*$_3$), 1.27 (s, 18H, C(C*H*$_3$)$_3$), 1.11 (d, J = 6.8, 24H, CH(C*H*$_3$)$_2$) ppm. ^{13}C NMR (101 MHz, C_6D_6): δ 168.04 (Ar*C*HN), 157.58 (Ar), 147.39 (Ar), 141.68 (Ar), 138.95 (Ar), 137.76 (Ar), 133.43 (Ar), 132.92 (Ar), 131.98 (Ar), 127.65

(Ar), 125.77 (Ar), 123.54 (Ar), 118.62 (Ar), 34.19 (Ar*C*(CH_3)$_3$), 31.57 (ArC(*C*H_3)$_3$), 28.67 (Ar*C*H(CH_3)$_2$), 23.46 (ArCH(*C*H_3)$_2$), 18.47 (Ar*C*H_3) ppm. HRMS (FAB+) Calcd. for $C_{56}H_{73}O_2N_2$: 805.5672. Found: 805.5688.

25-s—Metallation of **7-s** with $NiMe_2$(tmeda) was accomplished with the same procedure as the metallation of the *anti*-analog, though due to differences in solubility, the purification method was changed. After the reaction, volatiles were removed under vacuum and the resulting oily solid was dissolved in pentane and filtered over Celite to remove nickel(0). Precipitation from cold pentane yielded 0.20 g (73% yield) of ca. 92% pure desired complex. The remaining impurity was the mono-nickel complex. Subsequent precipitations yielded only minimal increase in purity. Analytically pure **25-s** was obtained by treating the nearly pure complex with half an equivalent of $NiMe_2$(tmeda) and 5 equivalents of pyridine using the same conditions as the initial reaction. Volatiles were removed under vacuum and the resulting oily solid was dissolved in pentane and filtered over Celite to remove nickel(0). Precipitation from cold pentane yielded 0.084 g (30% yield) of pure desired complex. X-ray quality crystals were grown from a cold pentane solution. ^{1}H NMR (400 MHz, C_6D_6): δ 8.00 (d, 4H, Py*H*), 7.66 (s, 2H, Ar*H*), 7.54 (m, 2H, Py*H*), 7.48 (s, 2H, Ar*H*), 7.16 (bs, 6H, N-Ar*H*), 7.10 (s, 2H, Ar*H*), 6.60 (m, 4H, Py*H*), 4.27 (septet, 4H, C*H*(CH_3)$_2$), 1.98 (s, 12H, ArC*H*$_3$), 1.53 (d, 12H, CH(C*H*$_3$)$_2$), 1.33 (s, 18H, C(C*H*$_3$)$_3$), 1.09 (d, 12H, CH(C*H*$_3$)$_2$), -0.75 (s, 6H, NiC*H*$_3$) ppm. ^{13}C NMR (101 MHz, C_6D_6): δ 166.62 (Ar*C*HN), 163.71 (Ar), 151.80 (Ar), 150.52 (Ar), 141.23 (Ar), 138.92 (Ar), 136.07 (Ar), 135.76 (Ar), 135.01 (Ar), 134.11 (Ar), 132.31 (Ar), 127.52 (Ar), 126.48 (Ar), 123.69 (Ar), 119.28 (Ar), 33.94 (Ar*C*(CH_3)$_3$), 31.66 (ArC(*C*H_3)$_3$), 28.65 (Ar*C*H(CH_3)$_2$), 25.05 (ArCH(*C*H_3)$_2$), 23.34 (ArCH(*C*H_3)$_2$), 18.70 (Ar*C*H_3), −7.33 (Ni*C*H_3) ppm. Anal. Calcd for $C_{68}H_{86}N_4Ni_2O_2$: C, 73.66; H, 7.82; N, 5.05. Found: C, 73.44; H, 7.66; N, 5.03.

General polymerization procedures

A 3 oz. Andrews glass pressure reaction vessel equipped with Swagelock valves and a gauge was used for all high pressure polymerizations. All polymerizations involving ethylene were carried out under the same conditions. The high-pressure setup was brought into the glove box with a magnetic stirbar and charged with the desired amounts of solvent and comonomer. A syringe was loaded with a solution of nickel complex and the needle was sealed with a rubber septum. The syringe and setup were brought out of the box and the setup was clamped firmly over a hot plate with a mineral oil bath previously regulated to 25 °C (or the desired temperature). The solution was stirred vigorously (1200 rpm). A nylon core hose equipped with quick connect adaptors was purged with ethylene for 1 minute and the pressure was set to 15 psi. The hose was connected to the setup and the setup was filled with ethylene. A bleed needle was inserted into a Teflon septum at the top of the high pressure setup and flushed with ethylene. The solution of nickel complex was added via syringe and the top of the setup was closed. The pressure was increased to 100 psi. After the desired time (generally 1 or 3 h), the ethylene hose was disconnected, the setup was vented and the reaction mixture was quenched with acidified methanol (3 times the reaction volume) to precipitate the polymer, which was collected as a white or pale yellow solid by filtration over a fine frit. If only a small amount of polymer was precipitated, the entire mixture was collected and volatile materials were removed under vacuum. Sample ^{1}H and ^{13}C NMR spectra are included in the SI.

Kinetic studies of 7-a isomerization

The four samples were prepared in the glove box by dissolving 0.044 g of **7-a** in 3.2 mL of 1-bromonaphthalene. 0.8 mL of the solution were transferred to each of four J Young tubes and sealed. These samples were brought out of the box and placed in preheated silicone oil baths at 140, 150, 160 and 170 °C. The samples at 140 and 150 °C were monitored at 30

minute intervals and the samples at 160 and 170 °C were monitored at 15 minute intervals by removing the sample from the bath, cooling to room temperature, and recording the d_0 ^{1}H NMR spectrum. The isomerization process was observed by comparing integration of the phenol peak, the isopropyl-methyne peak and the isopropyl-methyl peaks of the two isomers, which were distinguishable in the ^{1}H NMR spectrum (see SI for sample spectrum). The three values were averaged to determine the concentration for that time point. Time points were recorded until the reactions reached equilibrium. K_{eq} did not change between the four samples so that the final ratio of **7-s** and **7-a** was 0.61. The four plots of $\ln(X_e\text{-}X)$ versus time are included in the SI.

Supplementary Material

Refer to Web version on PubMed Central for supplementary material.

Acknowledgments

We thank Lawrence M. Henling (Caltech) for assistance with collection of crystallographic data and Jerzy Klosin (Dow Chemical) for the collection of GPC data. We are grateful to Dow Chemical and Caltech for funding. The Bruker KAPPA APEXII X-ray diffractometer was purchased via an NSF CRIF:MU Award to Caltech (CHE-0639094). The 400 MHz NMR spectrometer was purchased via an NIH award, RR027690.

References

1. Delferro M, Marks TJ. Chem Rev. 2011; 111:2450. [PubMed: 21329366]
2. Wilcox DE. Chem Rev. 1996; 96:2435. [PubMed: 11848832]
3. Lipscomb WN, Sträter N. Chem Rev. 1996; 96:2375. [PubMed: 11848831]
4. Cowan JA. Chem Rev. 1998; 98:1067. [PubMed: 11848925]
5. Li HB, Li LT, Schwartz DJ, Metz MV, Marks TJ, Liable-Sands L, Rheingold AL. J Am Chem Soc. 2005; 127:14756. [PubMed: 16231930]
6. Li HB, Marks TJ. Proceedings of the National Academy of Sciences of the United States of America. 2006; 103:15295. [PubMed: 17032766]
7. Rodriguez BA, Delferro M, Marks TJ. Organometallics. 2008; 27:2166.
8. Salata MR, Marks TJ. J Am Chem Soc. 2007; 130:12. [PubMed: 18076176]
9. Guo N, Li L, Marks TJ. J Am Chem Soc. 2004; 126:6542. [PubMed: 15161268]
10. Guo N, Stern CL, Marks TJ. J Am Chem Soc. 2008; 130:2246. [PubMed: 18220391]
11. Rodriguez BA, Delferro M, Marks TJ. Journal of the American Chemical Society. 2009; 131:5902. [PubMed: 19351155]
12. Makio H, Terao H, Iwashita A, Fujita T. Chem Rev. 2011; 111:2363. [PubMed: 21250670]
13. Younkin TR, Conner EF, Henderson JI, Friedrich SK, Grubbs RH, Bansleben DA. Science. 2000; 287:460. [PubMed: 10642541]
14. Bauers FM, Mecking S. Macromolecules. 2001; 34:1165.
15. Wehrmann P, Mecking S. Macromolecules. 2006; 39:5963.
16. Wehrmann P, Zuideveld M, Thomann R, Mecking S. Macromolecules. 2006; 39:5995.
17. Wehrmann P, Mecking S. Organometallics. 2008; 27:1399.
18. Hu T, Li YG, Li YS, Hu NH. J Mol Catal A-Chem. 2006; 253:155.
19. Na SJ, Joe DJ, Sujith S, Han WS, Kang SO, Lee BY. J Organomet Chem. 2006; 691:611.
20. Sujith S, Joe DJ, Na SJ, Park YW, Chow CH, Lee BY. Macromolecules. 2005; 38:10027.
21. Wang WH, Jin GX. Inorg Chem Commun. 2006; 9:548.
22. Zhang D, Jin GX. Inorg Chem Commun. 2006; 9:1322.
23. Chen Q, Yu J, Huang J. Organometallics. 2007; 26:617.
24. Hu T, Tang LM, Li XF, Li YS, Hu NH. Organometallics. 2005; 24:2628.

25. Kiesewetter ET, Randoll S, Radlauer M, Waymouth RM. J Am Chem Soc. 2010; 132:5566. [PubMed: 20359183]
26. Yan Y, Qin B, Shu YL, Chen XY, Yip YK, Zhang DW, Su HB, Zeng HQ. Org Lett. 2009; 11:1201. [PubMed: 19222182]
27. Kaur I, Jazdzyk M, Stein NN, Prusevich P, Miller GP. J Am Chem Soc. 2010; 132:1261. [PubMed: 20055388]
28. Wang CM, Friedrich S, Younkin TR, Li RT, Grubbs RH, Bansleben DA, Day MW. Organometallics. 1998; 17:3149.
29. Zysman-Colman E, Arias K, Siegel JS. Canadian Journal of Chemistry-Revue Canadienne De Chimie. 2009; 87:440.
30. Moore, JW.; Pearson, RG. Kinetics and Mechanism. 3. John Wiley & Sons; New York: 1981.
31. Lunazzi L, Mazzanti A, Minzoni M, Anderson JE. Org Lett. 2005; 7:1291. [PubMed: 15787489]
32. Hoogasian S, Bushweller CH, Anderson WG, Kingsley G. J Phys Chem. 1976; 80:643.
33. Gust D. J Am Chem Soc. 1977; 99:6980.
34. Zuideveld MA, Wehrmann P, Rohr C, Mecking S. Angewandte Chemie-International Edition. 2004; 43:869.
35. Janiak C. J Chem Soc, Dalton Trans. 2000:3885.
36. Connor EF, Younkin TR, Henderson JI, Hwang SJ, Grubbs RH, Roberts WP, Litzau JJ. Journal of Polymer Science Part a-Polymer Chemistry. 2002; 40:2842.
37. Gottker-Schnetmann I, Wehrmann P, Rohr C, Mecking S. Organometallics. 2007; 26:2348.
38. Crompton, TR. Analysis of Polymers: An Intoduction. Pargamon Press; 1989.
39. The extent of polymer branching was determined by 1H NMR spectroscopy.
40. Gates DP, Svejda SK, Onate E, Killian CM, Johnson LK, White PS, Brookhart M. Macromolecules. 2000; 33:2320.
41. Johnson LK, Killian CM, Brookhart M. J Am Chem Soc. 1995; 117:6414.
42. Gates DP, Svejda SA, Onate E, Killian CM, Johnson LK, White PS, Brookhart M. Macromolecules. 2000; 33:2320.
43. Mecking S, Johnson LK, Wang L, Brookhart M. J Am Chem Soc. 1998; 120:888.
44. Jenkins JC, Brookhart M. J Am Chem Soc. 2004; 126:5827. [PubMed: 15125675]
45. Schubbe R, Angermund K, Fink G, Goddard R. Macromol Chem Phys. 1995; 196:467.
46. Mecking reports both 1,2 and 2,1 insertions in α-olefin homopolymerizations, but indicates that this is in contrast with a report by Fink et al wherein they report only 1,2-insertions for a non-salicylaldiminato nickel system. Mecking suggests that the reason for this difference is steric crowding of the Ni center disfavoring 2,1 insertions. .
47. Klabunde U, Mulhaupt R, Herskovitz T, Janowicz AH, Calabrese J, Ittel SD. Journal of Polymer Science Part a-Polymer Chemistry. 1987; 25:1989.
48. Radlauer MR, Day MW, Agapie T. 2011 submitted.
49. Pangborn AB, Giardello MA, Grubbs RH, Rosen RK, Timmers FJ. Organometallics. 1996; 15:1518.
50. Berliner MA, Belecki K. Journal of Organic Chemistry. 2005; 70:9618. [PubMed: 16268645]
51. Kaschube W, Porschke KR, Wilke G. Journal of Organometallic Chemistry. 1988; 355:525.
52. Connor, EF.; Younkin, TR.; Henderson, JI.; Waltman, AW.; Grubbs, RH. Chemical Communications. 2003. p. 2272
53. Gorl C, Alt HG. Journal of Organometallic Chemistry. 2007; 692:5727.
54. Lodeiro S, Xiong QB, Wilson WK, Ivanova Y, Smith ML, May GS, Matsuda SPT. Organic Letters. 2009; 11:1241. [PubMed: 19216560]
55. Agapie T, Bercaw JE. Organometallics. 2007; 26:2957.
56. Akama T, Ishida H, Shida Y, Kimura U, Gomi K, Saito H, Fuse E, Kobayashi S, Yoda N, Kasai M. Journal of Medicinal Chemistry. 1997; 40:1894. [PubMed: 9191967]

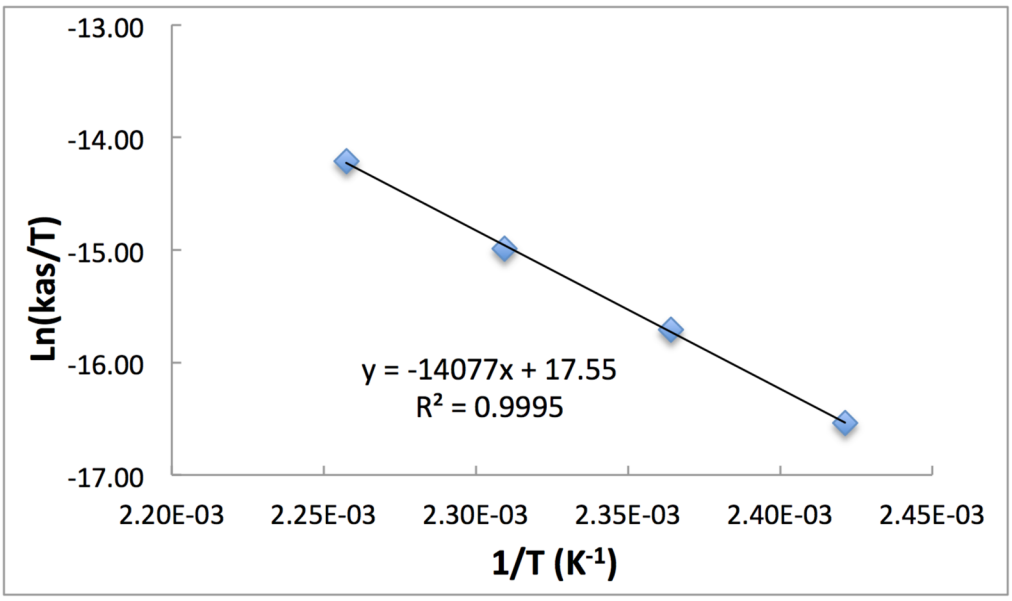

Figure 1.
Eyring plot for the isomerization of **7-a** to **7-s**.

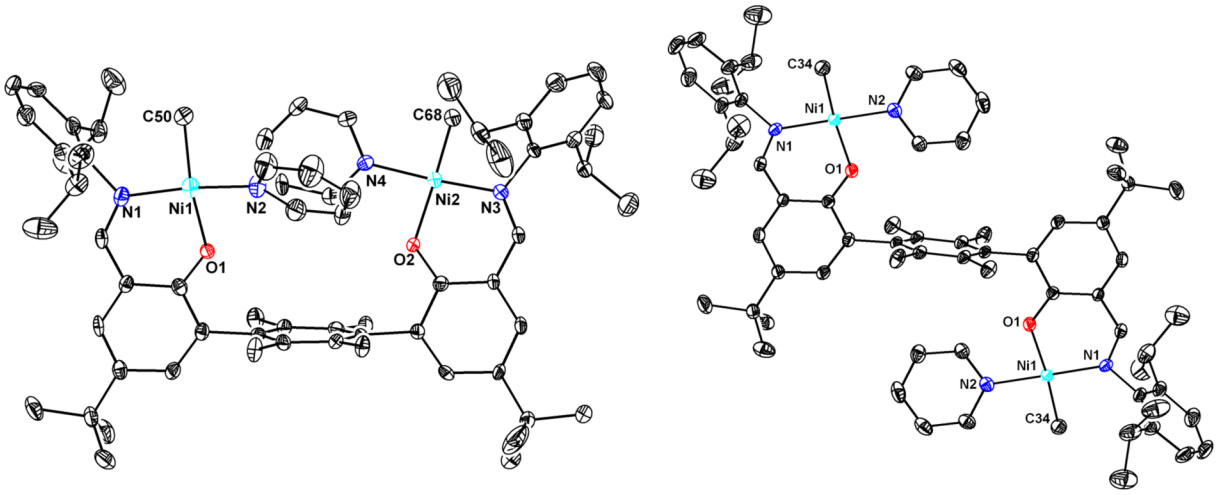

Figure 2.
Solid-state structures of **25-s** (left) and **25-a** (right) with thermal ellipsoids at the 50% probability level. For clarity, hydrogen atoms and solvent molecules are omitted.

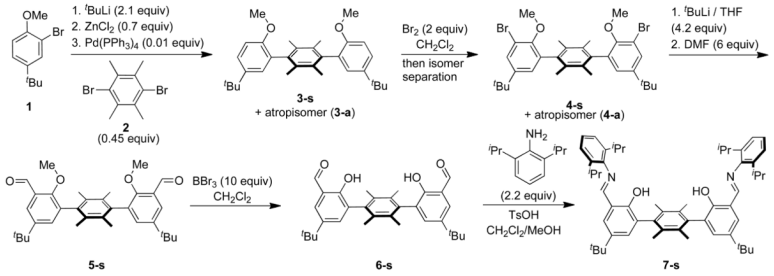

Scheme 1.
Synthesis of bis-salicylaldimine framework.

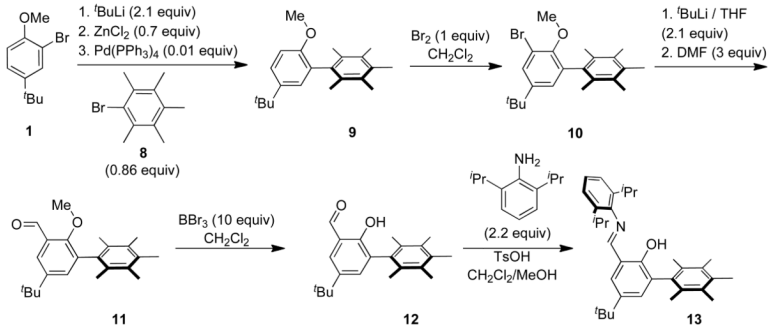

Scheme 2.
Synthesis of monucleating biphenyl-based salicylaldimine framework.

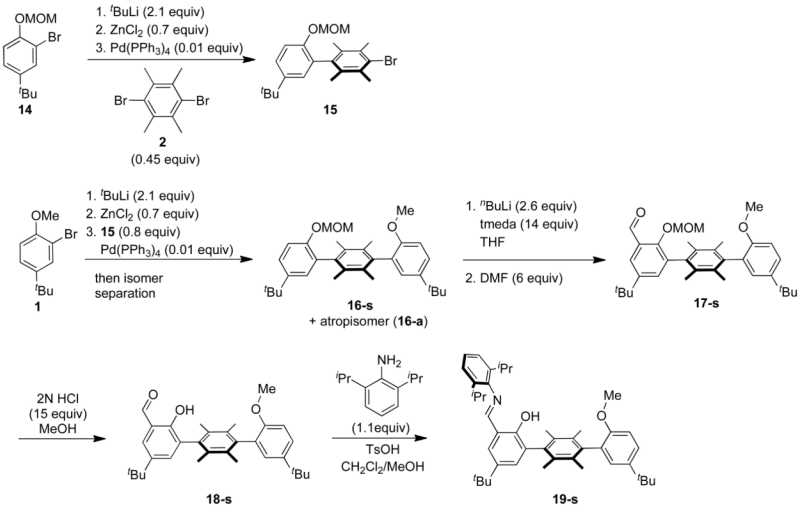

Scheme 3.

Synthesis of monucleating terphenyl-based salicylaldimine framework with methoxy substitution.

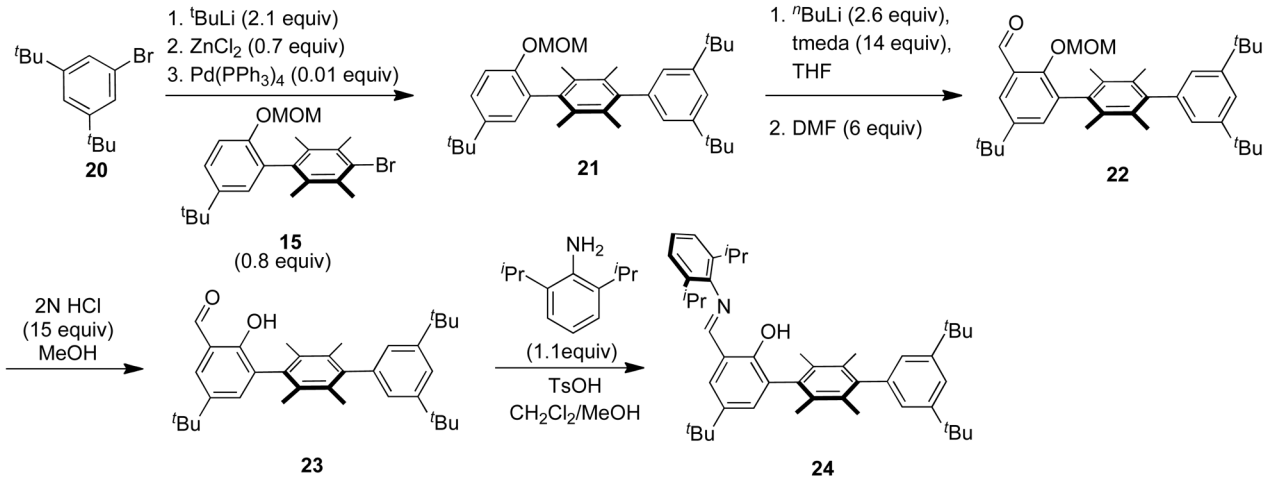

Scheme 4.

Synthesis of monucleating terphenyl-based salicylaldimine framework without methoxy substitution.

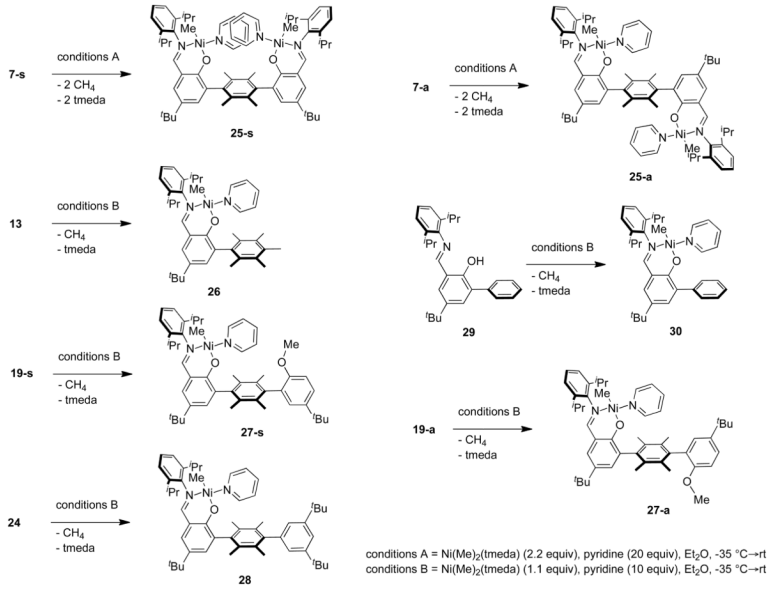

Scheme 5.
Synthesis of nickel complexes.

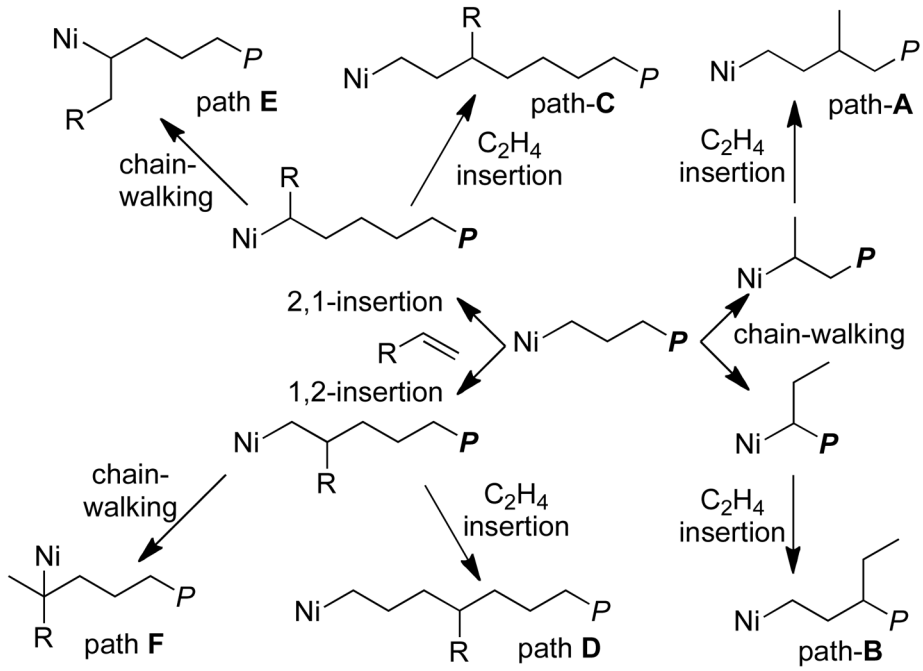

Scheme 6.
Insertion and chain walking processes during polymerization.

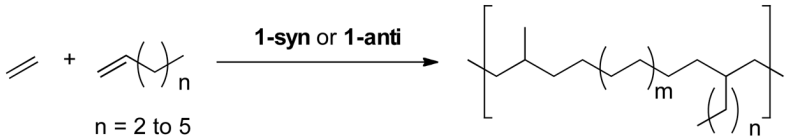

Scheme 7.
Copolymerizations of ethylene and α-olefins leads to only two types of branches.

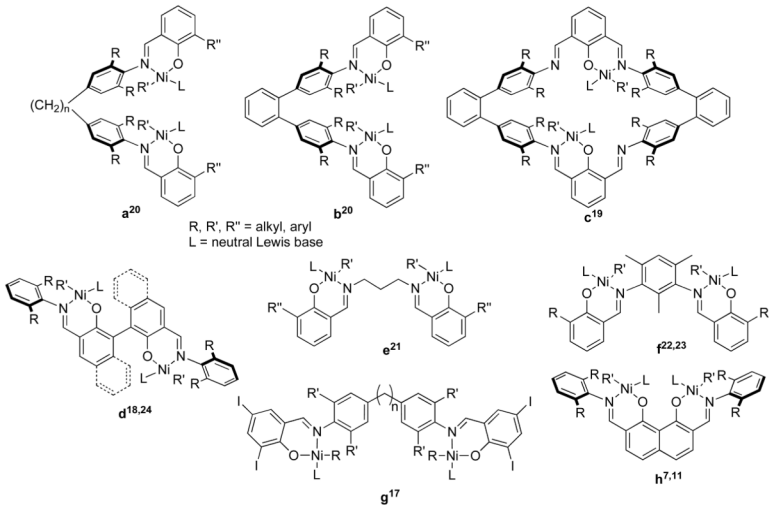

Chart 1.
Previously reported dinuclear nickel phenoxyiminato complexes.

Table 1

Ethylene homopolymerization trials.[a]

Entry	Complex	mmol Ni	Solvent	Volume (mL)	Time (h)	Yield	TOF[b]	Branching[c]
1	**25-a**	0.0126	toluene	25	1	0.680	1924	3.4
2	**25-a**	0.0126	toluene	25	1	0.940	2660	
3	**25-a**	0.0200	toluene	25	1	2.079	3705	
4	**25-a**	0.0200	toluene	25	3	3.415	2029	7.5
5	**25-a**	0.0200	toluene	25	1.5	1.893	2250	6.0
6[d]	**25-a**	0.0200	toluene	25	3	1.875	1114	
7	**25-a**	0.0080	toluene	5	3	0.118	280	
8	**25-a**	0.0080	THF	5	3	0.101	150	18.8
9	**25-a**	0.0080	THF	5	3	0.224	333	17.3
10	**25-s**	0.0126	toluene	25	1	0.150	424	25.5
11	**25-s**	0.0126	toluene	25	1	0.110	311	27.0
12	**25-s**	0.0200	toluene	25	3	0.574	341	19.6
13	**25-s**	0.0200	toluene	25	3	0.894	531	16.5
14	**25-s**	0.0080	toluene	5	3	0.047	69	
15	**25-s**	0.0080	toluene	5	3	0.036	53	
16	**25-s**	0.0080	THF	5	3	0.041	60	70.3
17	**25-s**	0.0080	THF	5	3	0.043	64	67.5
18	**26**	0.0200	toluene	25	3	5.532	3287	
19	**26**	0.0200	toluene	25	3	4.791	2846	
20	**26**	0.0080	toluene	5	3	0.549	815	
21	**26**	0.0080	THF	5	3	0.675	1003	7.2
22	**26**	0.0080	THF	5	1	0.172	766	8.4
23	**27-a**	0.0200	toluene	25	3	3.113	1850	3.8
24	**27-a**	0.0200	toluene	25	3	2.901	1724	5.1
25	**27-a**	0.0080	toluene	5	3	0.083	123	12.3
26	**27-a**	0.0080	THF	5	3	0.122	182	20.8

Entry	Complex	mmol Ni	Solvent	Volume (mL)	Time (h)	Yield	TOF[b]	Branching[c]
27	**27-a**	0.0080	THF	5	3	0.170	253	15.7
28	**27-s**	0.0200	toluene	25	3	1.205	716	3.8
29	**27-s**	0.0200	toluene	25	3	1.301	773	4.3
30	**27-s**	0.0080	toluene	5	3	0.047	70	9.6
31	**27-s**	0.0080	THF	5	3	0.037	54	26.8
32	**27-s**	0.0080	THF	5	3	0.041	61	27.2
33	**28**	0.0200	toluene	25	3	3.107	1846	
34	**28**	0.0080	toluene	5	3	0.100	148	10.8
35	**28**	0.0080	THF	5	3	0.099	147	19.6
36	**28**	0.0080	THF	5	3	0.081	121	19.6
37	**30**	0.0200	toluene	25	3	1.975	1174	
38	**30**	0.0200	toluene	25	3	2.879	1710	
39	**30**	0.0200	toluene	25	1	0.720	1284	
40	**30**	0.0080	toluene	5	3	0.416	618	
41	**30**	0.0080	THF	5	3	0.152	225	37.8
42	**30**	0.0080	THF	5	3	0.076	113	40.5

[a] All polymerizations were run in a glass reactor under 100 psig of ethylene at 25 °C.

[b] TOF = turnover frequency in (mol C_2H_4)×(mol Ni)$^{-1}$×h^{-1}.

[c] Branching was determined from ^{1}H NMR spectroscopy and is reported as the number of branches per 1000 carbons.

[d] In this polymerization, the stirring was reduced to one third of the rate used for all other polymerizations.

Table 2

Ethylene/1-hexene copolymerization trials.[a]

Entry	Complex	mmol Ni	Equiv hexene	Solvent	Volume (mL)	Temp (°C)	Time (h)	Yield (g)	TOF[b]	Branching[c]	Branch type[d]
1	**25-a**	0.0200	8000	toluene	25	25	1	0.107	191	36.3	m + b
2	**25-a**	0.0040	8000	toluene	5	25	3	0.030	89	49.1	m + b
3	**25-a**	0.0080	4000	toluene	5	25	3	0.043	64	33.0	m + b
4	**25-a**	0.0080	4000	THF	5	25	3	0.051	76	34.7	m + b
5	**25-a**	0.0080	3200	THF	5	25	3	0.112	167	31.1	m + b
6	**25-a**	0.0080	3200	THF	5	25	3	0.080	118	31.6	m + b
7	**25-s**	0.0040	8000	toluene	5	25	1	--[e]	--[e]	92.2	
8	**25-s**	0.0040	8000	toluene	5	25	3	0.020	59	76.6	m + b
9	**25-s**	0.0040	8000	toluene	5	25	12	0.016	12	65.2	m + b
10	**25-s**	0.0040	8000	toluene	5	25	12	0.040	30	78.4	m + b
11	**25-s**	0.0040	8000	toluene	5	40	3	0.012	36		
12	**25-s**	0.0040	8000	toluene	5	40	12	0.044	32		
13	**25-s**	0.0080	4000	toluene	5	25	3	0.023	34	54.0	m + b
14	**25-s**	0.0080	4000	toluene	5	25	3	0.017	25		
15	**25-s**	0.0080	3200	THF	5	25	3	0.018	26	63.7	m + b
16	**25-s**	0.0080	3200	THF	5	25	3	0.016	23	62.9	m + b
17	**26**	0.0080	3200	THF	5	25	3	0.193	287	32.8	m + b
18	**26**	0.0080	3200	THF	5	25	3	0.078	116	33.1	m + b
19	**27-a**	0.0080	3200	toluene	5	25	3	0.132	195	31.4	m + b
20	**27-a**	0.0080	3200	THF	5	25	3	0.092	136	34.8	m + b
21	**27-a**	0.0080	3200	THF	5	25	3	0.066	99	33.9	m + b
22	**27-s**	0.0080	3200	toluene	5	25	3	0.017	26	33.3	m + b
23	**27-s**	0.0080	3200	THF	5	25	3	0.028	42	38.9	m + b
24	**27-s**	0.0080	3200	THF	5	25	3	0.028	42	39.3	m + b
25	**28**	0.0080	3200	toluene	5	25	3	0.030	44	53.4	m + b

Entry	Complex	mmol Ni	Equiv hexene	Solvent	Volume (mL)	Temp (°C)	Time (h)	Yield (g)	TOF[b]	Branching[c]	Branch type[d]
26	**28**	0.0080	3200	THF	5	25	3	0.063	94	38.5	m + b
27	**28**	0.0080	3200	THF	5	25	3	0.108	160	38.8	m + b
28	**30**	0.0080	3200	THF	5	25	3	0.094	140	44.6	m + b
29	**30**	0.0080	3200	THF	5	25	3	0.047	70	48.4	m + b

[a] All polymerizations were run in a glass reactor under 100 psig of ethylene.

[b] TOF = turnover frequency in (mol C_2H_4)×(mol Ni)$^{-1}$×h^{-1}. This value is not adjusted for the amount of 1-hexene incorporated.

[c] Branching was determined from ^{1}H NMR spectroscopy and is reported as the number of branches per 1000 carbons.

[d] Determined from ^{13}C NMR spectroscopy: m = methyl, b = butyl.

[e] Too little polymer to accurately mass.

Table 3

Ethylene/α-olefin copolymerization trials with **25-a** and **25-s**.[a]

Entry	Complex	Comonomer	Yield (g)	Branching$_b$	Branch type[c]	Branch ratio[c]	% inc[d]	TOF e[e]	TOF co[e]	M_w[f]	M_n[f]	PDI[f]
1	**25-a**		0.101	17.3	m			150				
2	**25-a**		0.224	18.8	m			333		47591	6309	7.54
3	**25-s**		0.041	70.3	m			60				
4	**25-s**		0.043	67.5	m			64		8114	2697	3.01
5	**25-a**	1-pentene	0.087	33.4	m+p	1:1.7	4.5	123	2.3	15238	4271	3.57
6	**25-a**	1-pentene	0.086	31.3	m+p	1:1.5	4.0	123	2.0			
7	**25-s**	1-pentene	0.044	70.2	m+p	1:0.5	4.7	63	1.2	7707	2583	2.98
8	**25-s**	1-pentene	0.028	76.1	m+p	1:0.5	5.2	39	0.9			
9	**25-a**	1-hexene	0.112	31.1	m+b	1:2.5	4.9	159	2.7	14088	3712	3.80
10	**25-a**	1-hexene	0.080	31.6	m+b	1:2.9	5.2	112	2.0			
11	**25-s**	1-hexene	0.018	63.7	m+b	1:0.8	6.3	24	0.5			
12	**25-s**	1-hexene	0.016	62.9	m+b	1:0.5	4.8	22	0.4	2759	893	3.09
13	**25-a**	1-heptene	0.053	36.0	m+pn	1:3.4	6.5	74	1.5	9097	3037	3.00
14	**25-a**	1-heptene	0.045	40.7	m+pn	1:3.9	7.8	61	1.5			
15	**25-s**	1-heptene	0.022	68.0	m+pn	1:0.6	5.6	31	0.5	3619	1196	3.03
16	**25-s**	1-heptene	0.006	61.3								
17	**25-a**	1-octene	0.017	49.4	m+h	1:5.0	10.9	22	0.7	4472	1068	4.19
18	**25-a**	1-octene	0.017	49.5	m+h	1:8.0	11.9	22	0.7			
19	**25-s**	1-octene	0.012	61.0	m+h	1:0.8	6.7	17	0.3	2030	559	3.63
20	**25-s**	1-octene	0.009	51.1								
21	**25-a**	$C_{13}H_{24}O_2$[g]	0.037				2.7	45	1.3			
22	**25-s**	$C_{13}H_{24}O_2$[g]	0.002				1.6	1.7	0.03			

[a] All polymerizations were run for 3 h in a glass reactor with 0.0080 mmol of nickel in THF under 100 psig of ethylene with 3200 equivalents of comonomer at 25 °C. The total reaction volume was 5 mL.

[b] Branching was determined from ^{1}H NMR spectroscopy and is reported as the number of branches per 1000 carbons.

[c] Determined from ^{13}C NMR spectroscopy: m = methyl, p = propyl, b = butyl, pn = pentyl, h = hexyl.

[d] % incorporation was calculated from the overall branching and the branch ratio.

[e] TOF = turnover frequency in (mol monomer)×(mol Ni)$^{-1}$×h^{-1}. “e” = ethylene, “co” = comonomer. Calculated from the yield and the % incoporation of comonomer.

[f] Calculated from GPC results.

[g] Ethyl undecylenate; used 2500 equivalents (4.8 mL) with 0.2 mL THF for a total volume of 5 mL.